2012-02

Ethanol steam reforming over rhodium and cobalt-based catalysts: Effect of the support

INTERNATIONAL JOURNAL OF HYDROGEN ENERGY, OXFORD, v. 37, n. 4, pp. 3213-3224, FEB, 2012
http://www.producao.usp.br/handle/BDPI/34153

Available online at www.sciencedirect.com

SciVerse ScienceDirect

journal homepage: www.elsevier.com/locate/he

Ethanol steam reforming over rhodium and cobalt-based catalysts: Effect of the support

Jadson S. Moura [a], Marluce O.G. Souza [b], Jorge David A. Bellido [c], Elisabete M. Assaf [c], Marcelo Opportus [d], Patrício Reyes [d], Maria do Carmo Rangel [a,*]

[a] GECCAT – Grupo de Estudos em Cinética e Catálise, Instituto de Química, Universidade Federal da Bahia, Campus Universitário de Ondina, Federação, 40 170-280 Salvador, Bahia, Brazil

[b] Departamento de Ciências Exatas e da Terra, Universidade do Estado da Bahia, Campus I, Cabula. 41 195-001 Salvador, Bahia, Brazil

[c] Instituto de Química de São Carlos, Universidade de São Paulo, Av Trabalhador São Carlense, 13 560-970 São Carlos, São Paulo, Brazil

[d] Facultad de Ciencias Químicas, Universidad de Concepción, Casilla 160-C, Concepción, Chile

ARTICLE INFO

Article history:
Received 5 August 2011
Received in revised form
18 October 2011
Accepted 28 October 2011
Available online 9 December 2011

Keywords:
Hydrogen
Ethanol
Rhodium
Cobalt
Hydrotalcite
Steam reforming

ABSTRACT

The effect of support on the properties of rhodium and cobalt-based catalysts for ethanol steam reforming was studied in this work, by comparing the use of magnesia, alumina and Mg–Al oxide (obtained from hydrotalcite) as supports. It was found that metallic rhodium particles with around 2.4–2.6 nm were formed on all supports, but Mg–Al oxide led to the narrowest particles size distribution; cobalt was supposed to be located on the support, affecting its acidity. Rhodium interacts strongly with the support in the order: alumina> Mg–Al oxide > magnesia. The magnesium-containing catalysts showed low ethene selectivity and high hydrogen selectivity while the alumina-based ones showed high ethene selectivity, assigned to the Lewis sites of alumina. The Mg–Al oxide-supported rhodium and cobalt catalyst was the most promising sample to produce hydrogen by ethanol reforming, showing the highest hydrogen yield, low ethene selectivity and high specific surface area during reaction.

1. Introduction

The increasing demand for reducing the impact of modern life on the environment requires a continuous development of new technologies, aiming to reduce the pollutant emissions, mainly from automotive sources. Among them, the fuel cell fed by hydrogen is one of the most attractive options to obtain clean energy, since water is the only product of the reaction [1].

Therefore, an increase of hydrogen demand is expected due to fuel cells in a near future which, associated with the environmental restrictions for reducing air pollution and global emissions of greenhouse gases, requires the development of new routes for hydrogen production, especially from renewable sources. To fit these requirements, ethanol steam reforming reaction (Eq. (1)) emerges as the most convenient process, compared to the conventional methane steam reforming, partial oxidation of methane or methane dry reforming, due to the advantages of ethanol that include higher hydrogen content and availability, low toxicity and ease of storage and handling, as compared to methane. In contrast to fossil fuels, ethanol can be produced in

* Corresponding author. Tel.: +55 7132836867; fax: +55 7132355166.
E-mail address: mcarmov@ufba.br (M.C. Rangel).

0360-3199/$ – see front matter
doi:10.1016/j.ijhydene.2011.10.112

a renewable way from biomass, contributing to solve important environmental problems, such as the energy consumption and the dependency on fossil fuels. In addition, ethanol does not contribute to the increase of carbon dioxide emissions, since the carbon dioxide generated in the ethanol steam reforming is consumed during the biomass production.

$$C_2H_5OH_{(l)} + 3H_2O_{(l)} \rightarrow 6H_2(g) + 2CO_2(g) \quad \Delta H^0_{298K} = 347.4\,KJ\cdot mol^{-1} \tag{1}$$

A large amount of papers addressed to the production of hydrogen from ethanol involves the steam reforming process and catalysts based on noble metals, such as rhodium, platinum, iridium, palladium and ruthenium as well as non-noble metals, such as cobalt, nickel and copper [2–6]. Among noble metals, several studies showed that rhodium is the most active and selective one for the hydrogen production [7,8] while among the catalysts based on non-noble metals, those containing cobalt showed the highest activity and selectivity to hydrogen [9–12]. In fact, supported cobalt has shown similar activity to noble metals for the C–C bond cleavage, even around 400 °C, producing hydrogen from ethanol steam reforming [8,9].

It was noted by several authors [13–17] that the addition of promoters is very effective in improving the performance of catalysts for ethanol steam reforming. Promoters with alkaline properties, such as lithium, sodium, potassium, magnesium, lanthanum and cerium have been added to the catalysts with the primary purpose of inhibiting the deposition of coke during the reforming process, especially on nickel, copper and cobalt-based catalysts [15,16]. However it was observed, in some cases, that other properties were also improved, such as the decrease of reduction temperature and the increase of metallic dispersion. Moreover, the addition of a second and a third metal to nickel has also been studied and bimetallic catalysts, such as nickel and copper [18], nickel and cobalt [19] and nickel or cobalt promoted with noble metals [17] showed significant improvements, such as the increase of activity and selectivity to hydrogen and the ease of reduction to obtain the active phase.

Besides the metallic phase and the promoters, the support may also play a role on the properties of the catalysts for ethanol steam reforming. The use of basic supports, such as magnesium oxide [20] and lanthanum oxide [21], has shown to be a promising alternative to minimize coke deposition. However, their low specific surface areas lead to a low dispersion of the supported metal, which decrease the catalyst performance [8]. On the other hand, acid supports, such as gamma alumina, catalyze the dehydration of ethanol, causing an increased production of ethylene, which is pointed out [22] as the major precursor of coke in ethanol steam reforming.

Other properties of the solids have also been considered for choosing a support for ethanol steam reforming. Supports with high OSC (oxygen storage capacity) and high oxygen mobility, such as ceria and ceria-zirconia [13], seem to improve the catalyst stability, allowing the gasification/oxidation of coke just after its production. It was also observed that the use of aluminum and magnesium spinel [17] suppresses the formation of nickel or cobalt aluminate, making the metal reduction easier. Mesostructured solids were also used, allowing the control of pore size, pore volume and leading to high specific surface areas, which are important properties to accommodate the metallic particles. It was noted, for instance, that the use of SBA-15 material, as support of copper and nickel catalysts, increased their performance in ethanol steam reforming [15].

Aiming to obtain catalysts for ethanol steam reforming with improved properties, the effect of support on the properties of rhodium-based catalysts for ethanol steam reforming was studied in this work. Magnesia, alumina and Mg–Al oxide, obtained from hydrotalcite, were used as supports. The hydrotalcite-like compounds belong to the group of anionic clays, called layered double hydroxide. They have the general molecular formula $[M^{2+}_{1-x}M^{3+}_x(OH)_2]^{x+}(A_{x/n})^{n-}.mH_2O$, in which M^{2+} and M^{3+} are divalent and trivalent metal ions and A^{n-} is an anion intercalated in the structure. The thermal decomposition of these compounds produces oxides with properties suitable for applications in heterogeneous catalysis such as high specific surface area, basic surface properties, homogeneous distribution of the components and structural stability [23]. Moreover, in order to improve the catalysts performance, the effect of the addition of small amounts of cobalt on the properties of rhodium-based catalysts was also studied.

2. Material and methods

2.1. Samples preparation

In the preparation of hydrotalcites, magnesium and aluminum nitrates were dissolved in 250 mL of deionized water using a total cation concentration ($Al^{3+} + Mg^{2+}$) of 1.5 mol L^{-1} and a Mg^{2+} to Al^{3+} molar ratio of 2. This solution was added (1.5 mL min^{-1}) to 300 mL of a potassium carbonate solution and kept at 60 °C, under vigorous stirring. The required amount of potassium carbonate was calculated to obtain a ratio of $nCO_3^{2-} = 0.5\ nAl^{3+}$ and taken an excess of 10%. During the addition of solutions, the pH was maintained at 10 by the addition of a potassium hydroxide solution (2 mol L^{-1}). After precipitation, the system was kept under stirring for additional 2 h. The suspension was filtered and the solid was washed with deionized water at 60 °C, to eliminate potassium and nitrate ions. Then the material was dried at 75 °C, for 24 h, crushed and sieved in 80 mesh. The precursor thus obtained was calcined at 800 °C (to obtain stable supports), for 4 h, under air flow (100 mL min^{-1}). Pure magnesia and alumina were obtained by the same method.

The supports thus obtained were impregnated with solutions of rhodium nitrate and/or cobalt nitrate in order to obtain catalysts with 0.5% and 1% (weight) of rhodium and/or cobalt, respectively. The solids were dispersed in the solutions of the metal ions and kept at 70 °C, under stirring, until the evaporation of the solvent. After that, the sample was dried at 70 °C, for 16 h and calcined at 800 °C, for 2 h, under air flow (100 mL min^{-1}).

2.2. Samples characterization

The support precursors were characterized by thermogravimetry, differential thermal analysis and X-ray diffraction

while the supports were also analyzed by Fourier transform infrared spectroscopy of adsorbed pyridine. The fresh catalysts were characterized by elemental chemical analysis, Fourier transform infrared spectroscopy, X-ray diffraction, specific surface area measurements, temperature programmed reduction, transmission electron microscopy and electron diffraction. The spent catalysts were characterized by X-ray diffraction, specific surface area measurements and carbon measurements.

The thermogravimetry (TG) and differential thermal analysis (DTA) experiments were performed in a Mettler Toledo equipment, model TGA/SDTA 851. In the analysis, 0.005 g of sample was heated from 25 to 1000 °C, at a heating rate of 10 °C min^{-1}, under air flow (50 mL min^{-1}).

The contents of rhodium, cobalt, magnesium and aluminum in the catalysts were determined by inductively coupled plasma optical emission spectroscopy (ICP/OES), in a Vista Pro Simultaneous CCD Varian equipment. The samples containing aluminum were previously digested in a closed vessel, using a mixture of 25 mL of nitric acid and 75 mL of hydrochloric acid and heated at 150 °C, for 4 h. The samples without aluminum were digested using an aqueous solution of hydrochloric acid (50% v/v) in an open vessel at room temperature.

The Fourier transform infrared spectra (FTIR) were obtained in a Spectrum One Perkin–Elmer instrument. The samples were dispersed in potassium bromide and the spectra were collected using a resolution of 4 cm^{-1}, with an accumulation of 32 scans. The kinds of acid sites on the solids were identified by pyridine chemisorption. During the experiments, 0.070 g of sample was pressed (2 ton for 5 min) and transferred to a quartz cell equipped with potassium bromide windows. The sample was then outgassed in vacuum at 120 °C, for 1 h and then the background spectrum was recorded. After that the samples were kept in contact with pyridine vapor (5 mbar for 5 min) and a new spectrum was collected, subtracting the background.

The X-ray diffraction (XRD) analysis was carried out in an XRD 6000 Shimadzu equipment, using CuKα radiation generated at 40 kV and 30 mA, with a nickel filter. The data were collected over a 2θ range of 5–80°, with a step size of 0.02°, at a scanning rate of 2°.min^{-1}. The hydrotalcite stability upon heating was monitored by getting X-ray diffractograms at different temperatures (25, 100, 200, 300, 400, 500, 600, 700, 800, 900 and 1000 °C) heating the samples in situ in a chamber. The solids were heated at a rate of 10°min^{-1} under air (20% O_2, 80% N_2) flow (100 mL min^{-1}) up to the desired temperature, kept for 1 h at this temperature and the spectrum was registered. This procedure was repeated at each temperature.

The specific surface area measurements and the experiments of temperature programmed reduction (TPR) were carried out in a TPD/TPR 2900 Micromeritics instrument. In the first case, 0.150 g of sample was previously heated (10 °C min^{-1}) up to 160 °C, keeping the sample at this temperature for 30 min under nitrogen flow (60 ml min^{-1}). The specific surface area measurements were performed by nitrogen physisorption, using a mixture of 30% of nitrogen in helium, at liquid nitrogen temperature (−196 °C), using the BET method. In the experiments of temperature programmed reduction, the sample was heated up to 1000 °C (10 °C min^{-1}), under a flow of a mixture of 15% of hydrogen in nitrogen (50 ml min^{-1}).

The transmission electron micrographs (TEM) and the electron diffraction (ED) patterns were obtained in a Jeol model JEM 1200 EXII microscope. Before analysis, samples were reduced in a separated oven, for 1 h at 800 °C, under hydrogen flow (100 mL min^{-1}). The ground samples were dispersed in ethanol and drops of each dispersion were placed on copper grids. The micrographs were obtained in both bright and dark fields. For ED studies, 120 kV and 60 cm were used as acceleration voltage and focus distance, respectively. Aluminum was used as standard for calibration.

2.3. Catalytic evaluation

The catalysts were evaluated in ethanol steam reforming in a fixed bed tubular quartz reactor, containing 0.150 g of the sample. The experiments were carried out under atmospheric pressure, at 500 °C, for 6 h. Before reaction, the catalyst was reduced in situ at 800 °C, for 1 h, under hydrogen flow (30 mL min^{-1}). During reaction, a mixture of water and ethanol (molar ratio of 3:1) was fed to the reactor by a pump (2.5 mL h^{-1}). The gaseous reaction products (hydrogen, carbon dioxide, carbon monoxide, methane and ethene) were analyzed on-line, using a CG-3800 Varian gas chromatograph, equipped with Porapack N and molecular sieve 13X columns. The liquid products and the remaining reagents were collected into a container kept inside an ice bath and then analyzed in a 5890 Hewlett Packard chromatograph, equipped with an FFAP capillary column.

The selectivity (%) of the catalysts to *i* product was calculated according Eq. (2) and the yield of *i* product was calculated according Eq. (3).

$$Si(\%) = \frac{Fmol(i\ product)}{\sum Fmol(products)} \times 100 \quad (2)$$

where:

S_i (%) = selectivity to the *i* product

Fmol (i product) = molar flow of i product

$\sum$ Fmol (products) = sum of the molar flows of all products

$$Y_i(\%) = \frac{X_{EtOH}(\%) \times Si(\%)}{100} \quad (3)$$

where:

Y_i (%) = yield of *i* product

X_{EtOH} (%) = ethanol conversion

S_i (%) = selectivity to *i* product

3. Results and discussion

3.1. Catalysts characterization

Fig. 1 displays the TG curves of the support precursors. The magnesium-based precursor showed a strong weight loss (290–430 °C), assigned to magnesia production [24] and a small weight loss (430–650 °C) due to decomposition of the largest particles. The alumina-based precursor showed

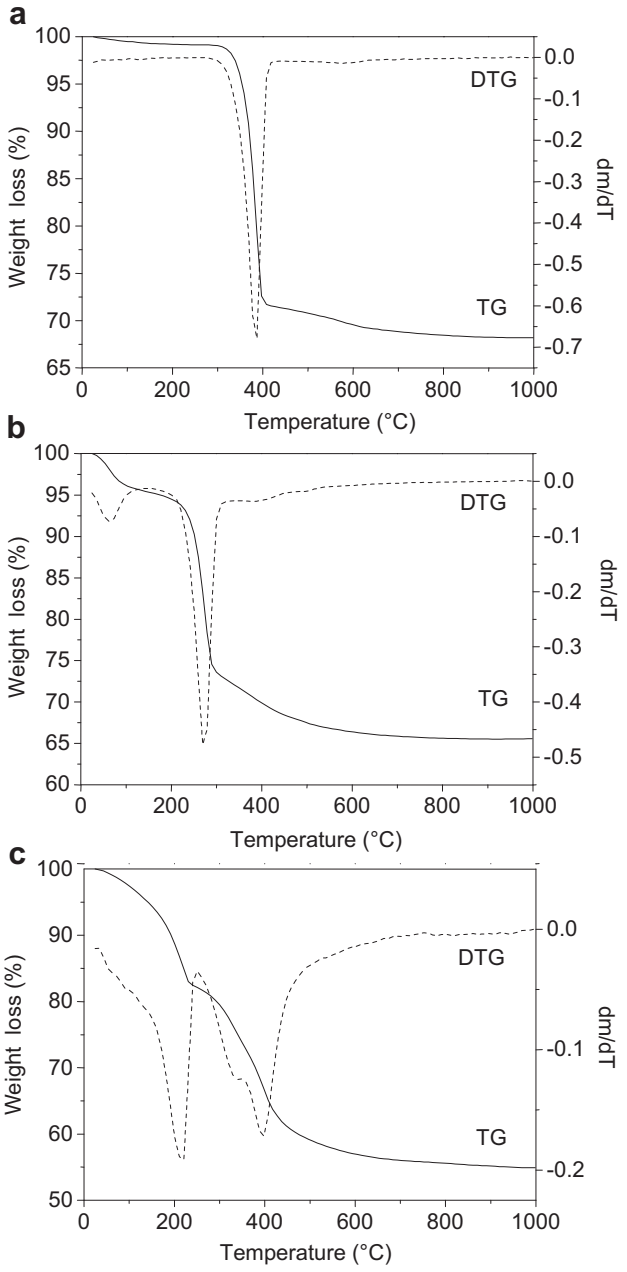

Fig. 1 – Thermogravimetry (TG) and derivative thermogravimetry (DTG) curves for the support precursors. (a) PM, (b) PA and (c) PAM samples: precursors of magnesia, alumina and of aluminum and magnesium-based solid, respectively.

a weight loss (200–320 °C) associated to alumina production and another one (320–480 °C), due to decomposition of bohemite. A typical curve of hydrotalcite decomposition was obtained for the PAM sample (Fig. 1c), in which the event at 150–260 °C is due to the loss of water from the interlayer spaces of the structure [23]. The peak at 339 °C (DTG curve) is related to the beginning of hydroxide layers decomposition and the third loss, associated to a peak centered at 398 °C in DTG curve, is due to the end of decomposition of hydroxide layers and of carbonate ions, also present in the interlayer spaces [23]. A small weight loss, at temperatures above 500 °C, is due to the decomposition of nitrate ions in the solid [25]. All these processes are endothermic ones, as shown by the DTA results (Fig. 2).

The FTIR spectra of the supports indicated the presence of adsorbed carbonate ions (Fig. 3), by the bands at 1444 cm^{-1} (M sample), 1390 cm^{-1} and 1520 cm^{-1} (A sample) and at 1380 cm^{-1} (MA sample), which are typical of basic solids [25]. The broad band over 3000 cm^{-1} is due to vibrations of hydroxyl groups while the band at 1637–1650 cm^{-1} is assigned to the angular vibration of water molecules on the surface [25]. The bands at 666 and 788 cm^{-1} are related to Al–O bonds while that at 447 cm^{-1} is due to Mg–O bonds [25].

The surface acid sites were identified by the FTIR spectra of adsorbed pyridine on alumina and magnesia supports, which are supposed to have the most different properties. Fig. 4 shows that alumina exhibits essentially Lewis acidity while magnesia showed acidity much lower than alumina, as expected. The bands at 1593 (1595), 1490 (1482) cm^{-1}, 1452 cm^{-1} and 1446 (1441) cm^{-1} are assigned to pyridine adsorbed on Lewis sites of alumina (or magnesia) [26]. The lack of bands at 1640 and 1545-1540 cm^{-1} for both solids indicates the absence of Brönsted acidity or that these acid sites are not strong enough to interact with pyridine and generate the pyridinium ions [26].

The X-ray diffractograms for the support precursors are shown in Fig. 5. The profile for the PAM sample is characteristic of hydrotalcite (JCPDS 14-0191), in accordance with the TG result. For the magnesium-free sample, the structure of bayerite, α-$Al(OH)_3$ (JCPDS 20-0011), was obtained. Regarding the aluminum-free solid, the structure of brucite ($Mg(OH)_2$) was produced (JCPDS 07-0239).

Fig. 6 shows the X-ray diffractograms of hydrotalcite taken after heating in situ at different temperatures. The solid is decomposed between 200 and 400 °C generating magnesium oxide, in accordance with previous work [25]. From 400 to 800 °C, no other crystalline phase was identified. At 900 °C, the

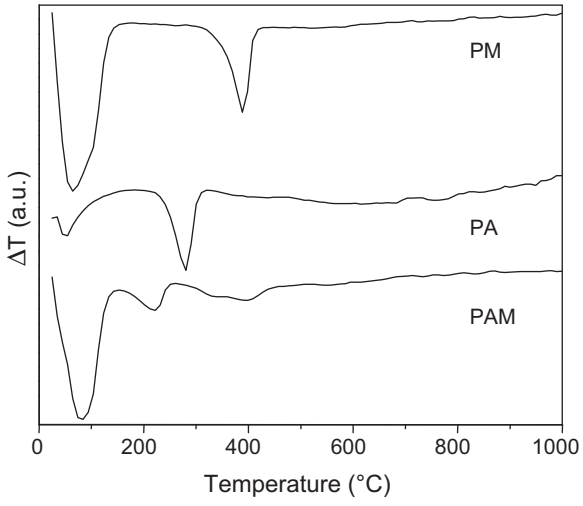

Fig. 2 – Differential thermal analysis (DTA) curves for the support precursors. PM, PA and PAM samples: precursors of magnesia, alumina and of aluminum and magnesium-based solid, respectively.

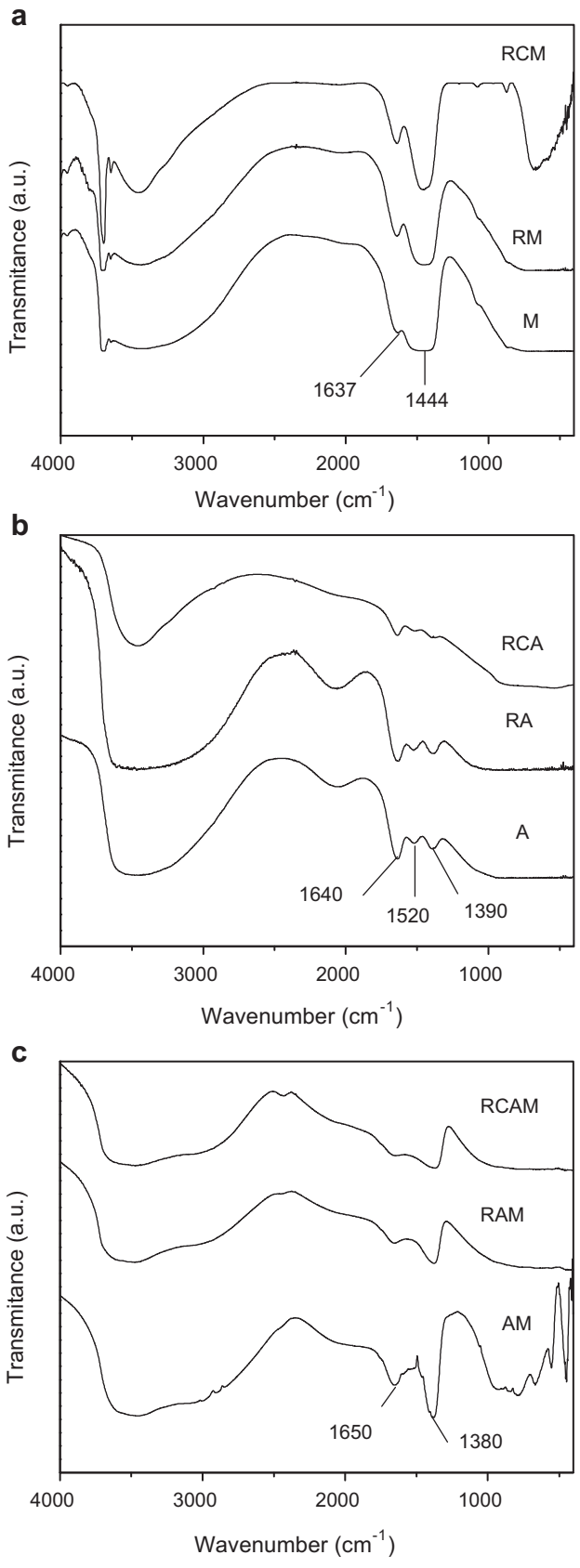

Fig. 3 – Fourier transform infrared spectra for the supports and for the catalysts based on (a) magnesia (M), (b) alumina (A) and (c) aluminum and magnesium-based solid (AM). R: rhodium; C: cobalt.

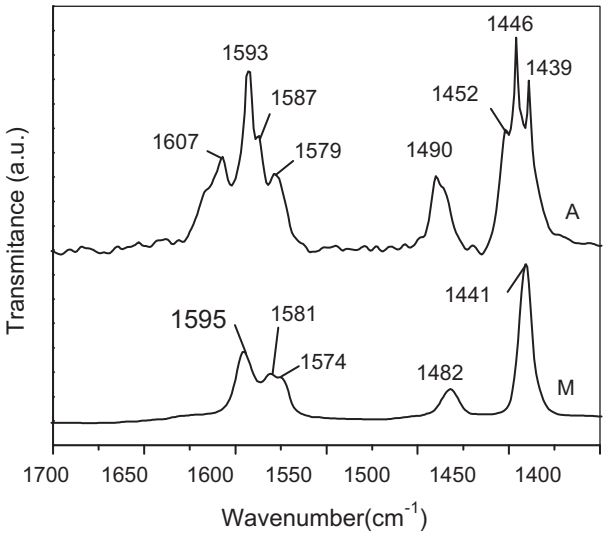

Fig. 4 – Fourier transform infrared spectra of adsorbed pyridine on the supports. A: alumina; M: magnesia.

aluminum and magnesium spinel ($MgAl_2O_4$) appeared, which is stable up to 1000 °C, as found previously [4].

The X-ray diffractograms of the catalysts based on magnesia (Fig. 7a) show the presence of magnesia (JCPDS 87-0653) and magnesium hydroxide (JCPDS 07-0239) for all samples. In the case of the alumina-based catalysts (Fig. 7b), peaks associated to gamma alumina (JCPDS 10-0425) were found while the catalysts originated from hydrotalcite showed peaks related to magnesia (JCPDS 87-0653) and to aluminum and magnesium spinel, $MgAl_2O_4$ (JCPDS 05-0672) (Fig. 7c). The spinel formation was attributed to calcination carried out at high temperature (800 °C), for 4 h. As shown in Fig. 6, heating for 1 h is not enough to produce the spinel structure at this temperature. The spent catalysts showed the

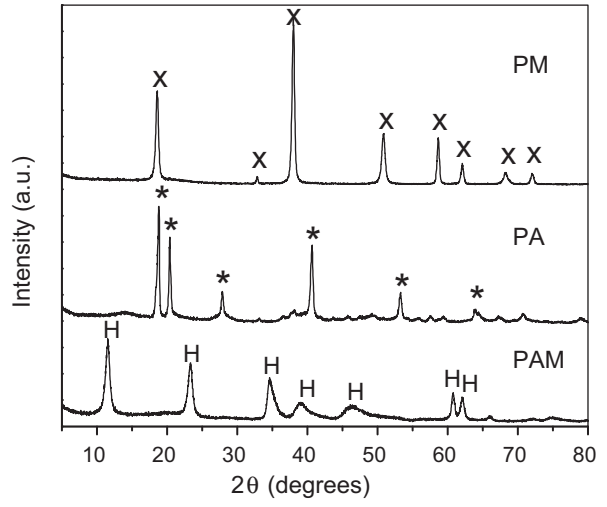

Fig. 5 – X-ray diffractograms for the support precursors. PM, PA and PAM samples: precursors of magnesia, alumina and aluminum and magnesium-based solid, respectively. X: $Mg(OH)_2$; *: $Al(OH)_3$; H: hydrotalcite.

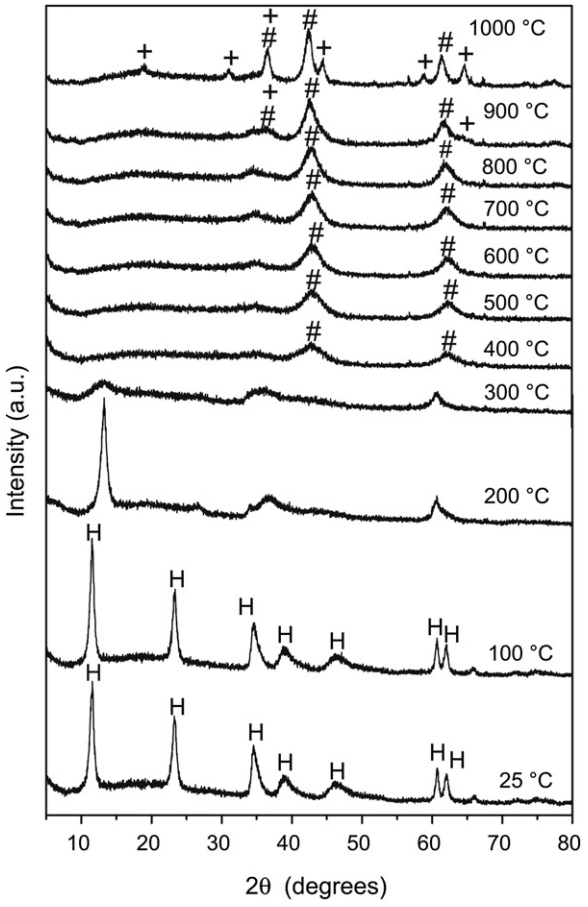

Fig. 6 – X-ray diffractograms of hydrotalcite (PAM sample) upon heating. H: hydrotalcite; #: MgO; +: $MgAl_2O_4$.

same phases as the fresh ones, indicating that all catalysts were stable during ethanol steam reforming, as shown in Fig. 8.

The contents of rhodium and cobalt were close to the nominal values, as well as the values of the Mg/Al ratio (equal to 2), as shown in Table 1. As expected, alumina-based catalysts showed higher specific surface areas as compared to magnesia-based ones (Table 1), regardless the presence of cobalt. Magnesium and aluminum-based solid showed different values depending on the presence of cobalt; for the rhodium-based sample, an intermediate value was found, which is close to the alumina-supported rhodium one; however, both cobalt and rhodium led to a solid with specific surface area higher than the alumina-based catalysts. It suggested that the impregnation with both cobalt and rhodium, followed by calcination at high temperatures, caused textural changes resulting in an increase of specific surface area. After reaction, the solids showed lower values, indicating that they went on sintering during the reduction step and/or during ethanol steam reforming. This sintering is probably related to the reaction medium, since the samples were previously calcined at 800 °C and then reduced at the same temperature.

Magnesium and aluminum oxide-supported rhodium showed the highest decrease of specific surface area during reaction, reaching a value as low as 8.0 $m^2\ g^{-1}$. This sintering

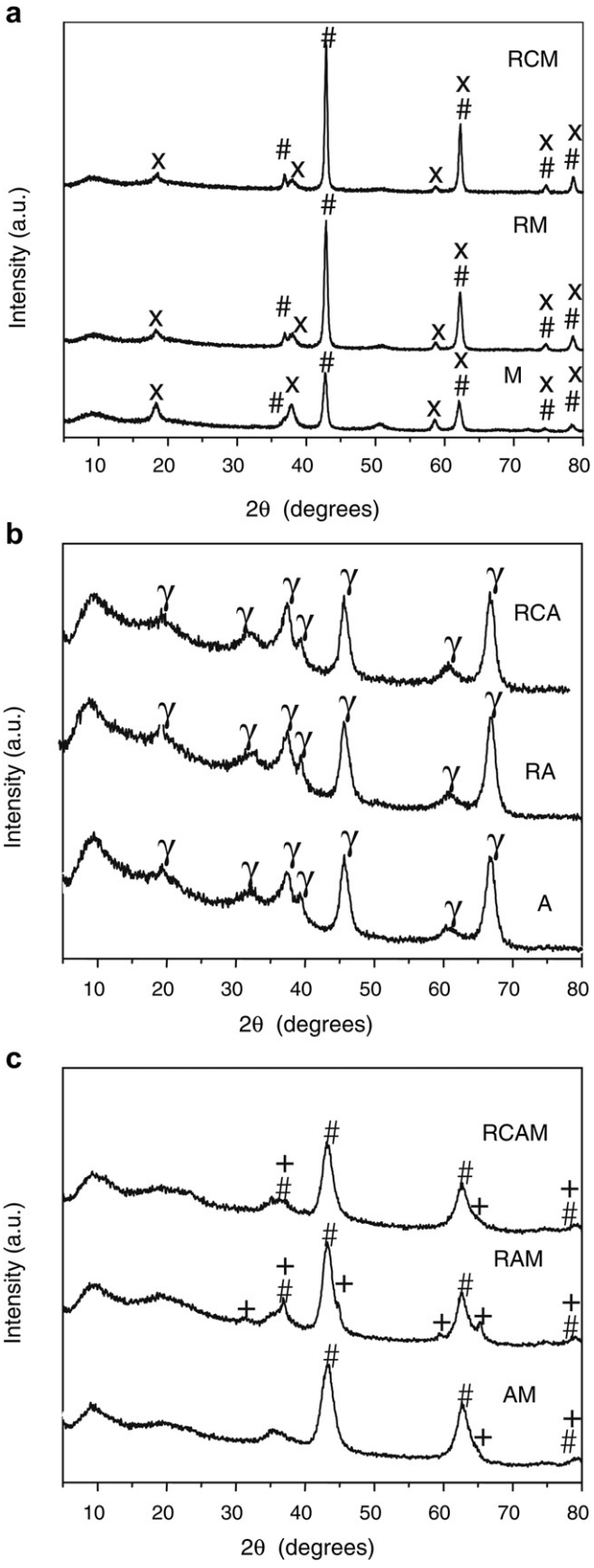

Fig. 7 – X-ray diffractograms of fresh catalysts based on (a) magnesia (M), (b) alumina (A) and (c) aluminum and magnesium-based solid (AM). R: rhodium; C: cobalt. #: MgO; X: $Mg(OH)_2$; γ : γ-Al_2O_3; +: $MgAl_2O_4$.

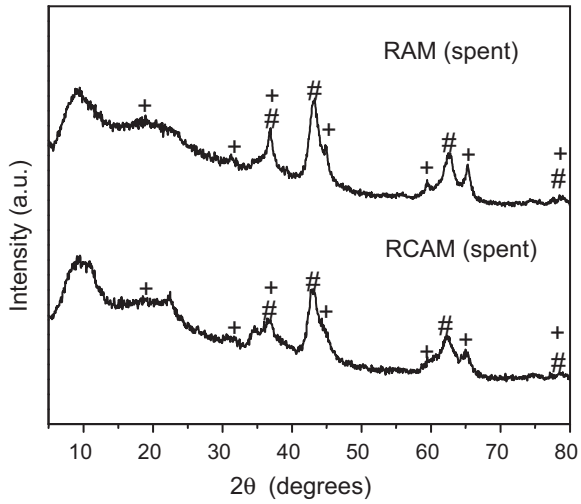

Fig. 8 – X-ray diffractograms of spent catalysts based on aluminum and magnesium-based solid (AM sample). R: rhodium; C: cobalt; #: MgO; +: $MgAl_2O_4$.

is probably related to the presence of steam which is a well-known plasticizing agent, favoring sintering [27]. The addition of cobalt, however, seems to delay sintering under ethanol reforming and a higher value was shown by the corresponding sample containing cobalt (101 $m^2 g^{-1}$). This finding was also noted for other supports and may be related to phase changes in the solid. It is known [17] that cobalt can form a stable solid solution CoO–MgO or stable compounds such cobalt aluminate at high temperatures; the blue color of the RCA sample confirmed the production of this compound.

The TPR curve for magnesia (Fig. 9a) showed a peak at 398 °C due to carbonate species on the surface, as previously reported [28]. The shoulder at 398 °C (RM sample) and the peak at 395 °C (RCM sample) are assigned to this process; however, they can also be related to non-stochiometric rhodium oxide (RhO_x) [29]. The RM and RCM samples showed other peaks at 453 and 458 °C, respectively, due to non-stochiometric rhodium oxide (RhO_x) in strong interaction with the support [29], generated at 800 °C.

As expected, alumina did not show any reduction peak (Fig. 9b). The RA sample showed a peak at 356 °C, due to rhodium oxide (RhO_x) [29]. Above this temperature, only

Table 1 – Elemental chemical composition and specific surface area of the catalysts before (Sg) and after (Sg*) ethanol steam reforming.

Sample	Rh (% w/w)	Co (% w/w)	Mg/Al (molar)	Sg ($m^2 g^{-1}$)	Sg* ($m^2.g^{-1}$)
RA	0.55 ± 0.01	–	–	142	113
RAM	0.47 ± 0.01	–	2.0 ± 0.1	114	8.0
RM	0.47 ± 0.01	–	–	61	27
RCA	0.59 ± 0.01	1.10 ± 0.01	–	145	126
RCAM	0.43 ± 0.02	0.82 ± 0.01	2.0 ± 0.1	175	101
RCM	0.49 ± 0.01	1.10 ± 0.01	–	56	43

R: rhodium; C: cobalt; M: magnesia; A: alumina; AM: aluminum and magnesium-based solid.

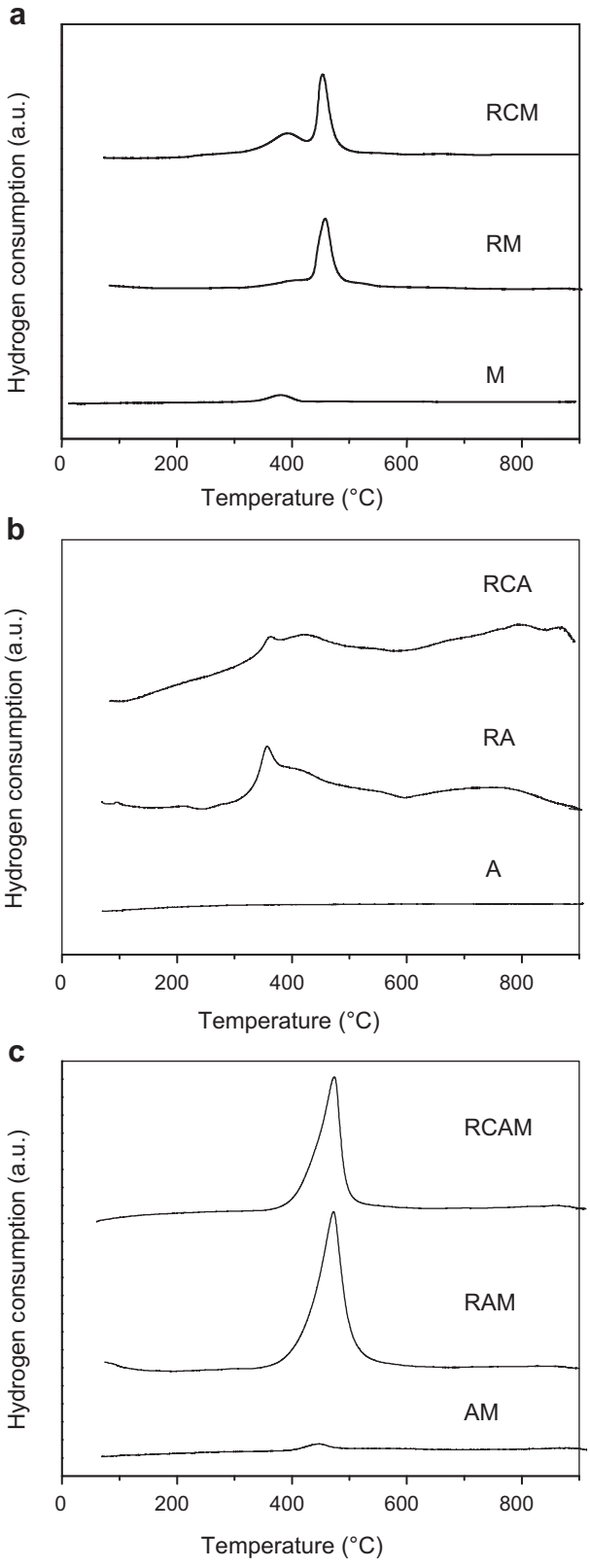

Fig. 9 – Temperature programmed reduction curves of fresh catalysts based on (a) magnesia (M); (b) alumina (A) and (c) on aluminum and magnesium-based solid (AM). R: rhodium; C: cobalt.

a broad and poorly defined peak was observed. This finding is in agreement with a previous work [30], according to which, during calcination of alumina-supported rhodium catalysts at high temperatures, rhodium oxide particles go into the defects on alumina surface and become highly bonded, producing stable species, difficult to reduce. A similar profile was shown by the RCA sample; in this case, only a broad and poorly defined reduction peak was found; the shoulder at 364 °C is related to rhodium oxide (RhOx).

For samples generated from hydrotalcite (Fig. 9c), the AM sample showed a small reduction peak at 449 °C, assigned to surface carbonates species [28]. The RAM sample showed an intense peak at 472 °C, due to the reduction of rhodium oxide ($RhOx_x$) in interaction with the support [29]. A similar profile was shown by the RCAM sample, with an intense peak at 474 °C, also related to rhodium oxide (RhO_x) reduction [29].

The TPR curves of cobalt monometallic catalysts (not shown) confirmed that this metal is non reducible up to 800 °C. This is probably due to the production of cobalt aluminate and/or the solid solution CoO–MgO, as detected by X-ray diffraction (not shown), which are reduced only at high temperatures, in agreement with a previous work [17].

Fig. 10 shows the TEM images of rhodium-containing samples after reduction. The micrographs reveal small metal particles, which can be related to the strong interaction between rhodium and the support, as detected by TPR. The interplanar distances of the RA and RCAM samples, calculated from the electron diffraction patterns, were characteristic to (111), (200), (220) and (222) planes of metallic rhodium. The RAM sample did not show any diffraction pattern. No alloy

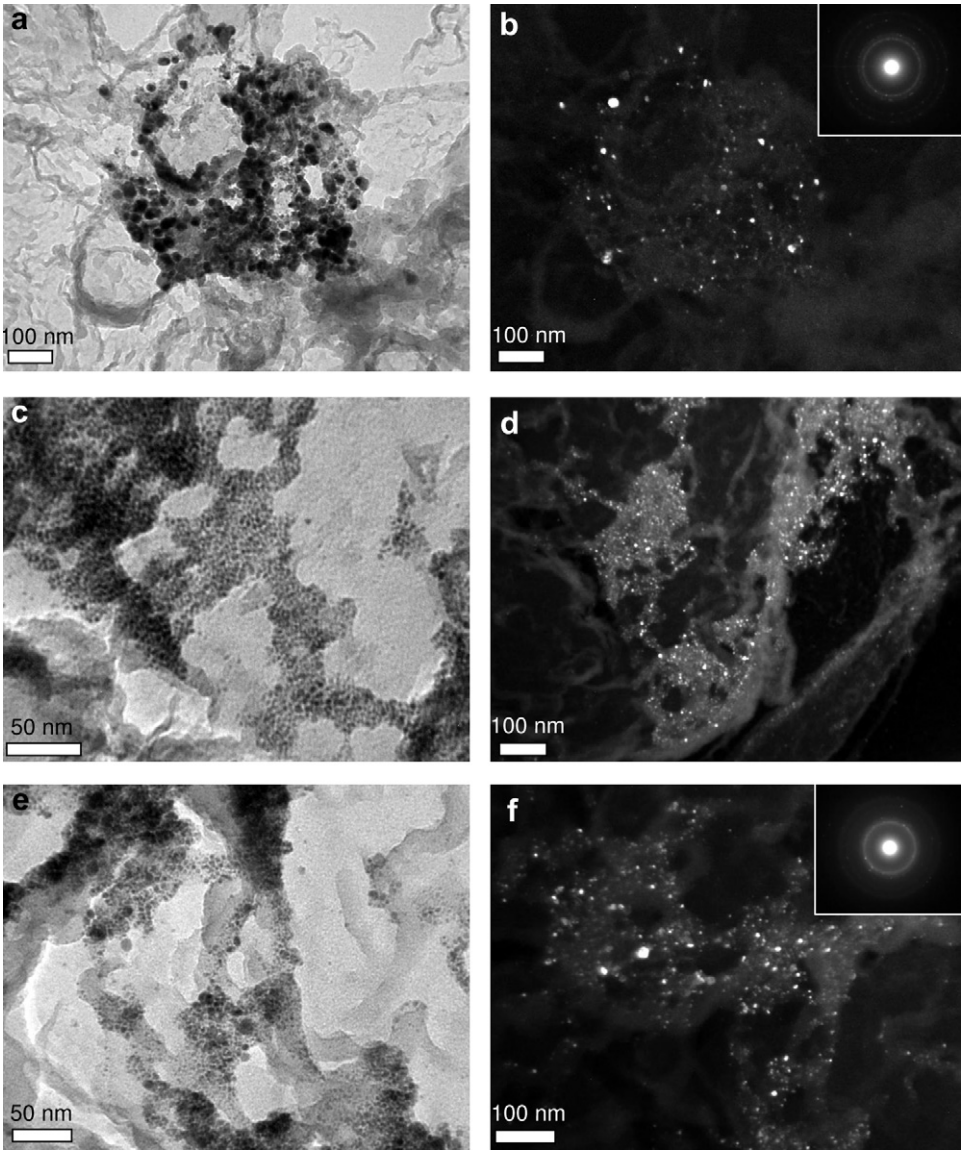

Fig. 10 – Transmission electron micrographs of the reduced catalysts. RA (a, b), RAM (c, d) and RCAM (e, f) taken on bright field (a, c, e) and on dark field (b, d, f) and electron diffraction patterns of rhodium particles on RA (inset at b) and RCAM samples (inset at f). RA: alumina-supported rhodium; RAM: of aluminum and magnesium solid-supported rhodium; RCAM: aluminum and magnesium oxide-supported rhodium and cobalt.

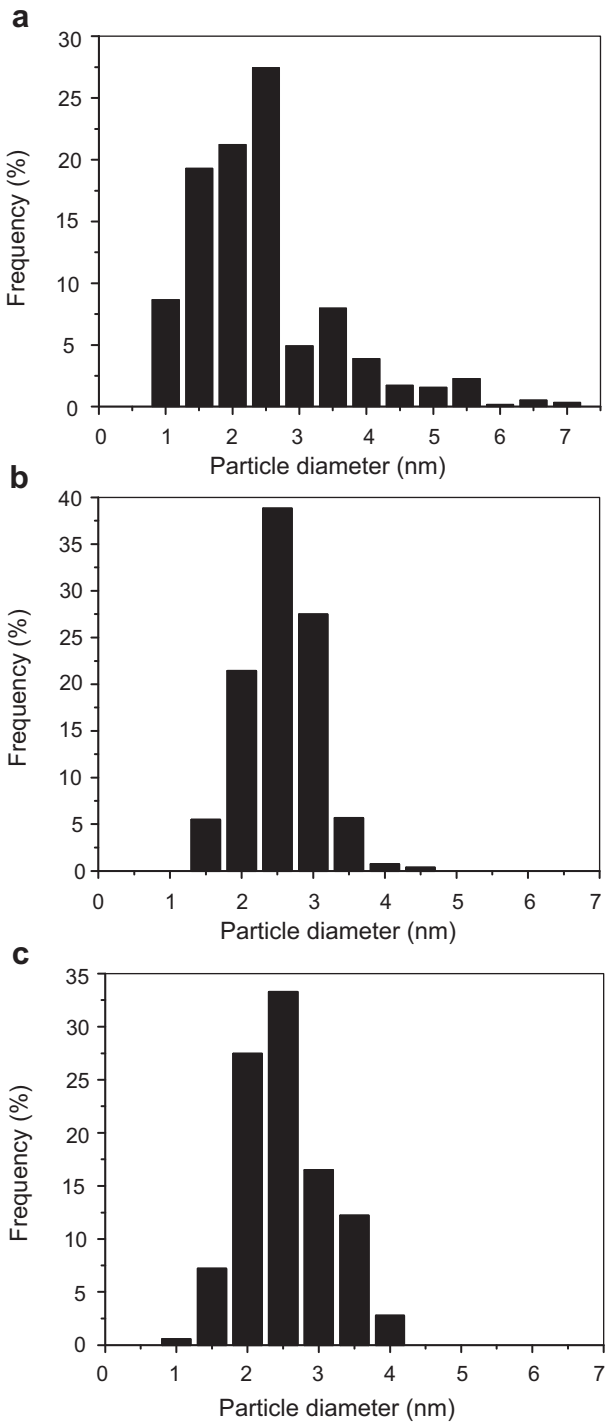

Fig. 11 – Rhodium particles size distribution obtained by TEM for the reduced catalysts. (a) alumina-supported rhodium (RA); (b) Mg–Al oxide-supported rhodium (RAM) and (c) of Mg–Al oxide-supported rhodium and cobalt (RCAM sample).

between rhodium and cobalt was detected in any sample, suggesting that cobalt is interacting with the support.

The average particles size was similar for all samples: 2.4 nm (RA sample), 2.6 nm (RAM) and 2.6 nm (RCAM). The production of such small particles can be assigned to the strong interaction between rhodium and the supports, as found by TPR. However, from Fig. 11, one can see that different particles size distributions for rhodium particles were obtained, as the consequence of the different supports. Alumina led to the broadest distribution of particles size, ranging from 1 to 7 nm while magnesium led to a narrower distribution ranging from 1.5 to 4.5 nm; the presence of both magnesium and cobalt led to a similar distribution ranging from 1 to 4 nm. Moreover, the particles size distribution is shifted to smaller diameters for RA sample (Fig. 11a), indicating that most of particles is smaller than 2.5 nm. This finding is in agreement with the TPR results, which showed that rhodium particles are in the strongest interaction with alumina and thus the production of the smallest particles is favored. On the other hand, the interaction between rhodium and Mg–Al oxide is weaker than alumina and then the distribution is shifted to bigger sizes for the RAM sample (Fig. 11b). For the RCAM sample, the distribution is intermediate between the other ones, indicating that cobalt favors the production of small particles.

3.2. *Catalysts evaluation*

The RA and RCA samples led to the highest conversions (Table 2), a fact that can be attributed to the additional activity of alumina for ethanol dehydration reaction (Eq. (4)) [22], as shown by the highest ethene selectivities of RA and RCA samples. The addition of cobalt decreased the conversion due to a decrease of ethene selectivity, indicating a decrease of the acidity of the support. These results are closely related to the presence of Lewis sites on alumina, as detected by pyridine chemisorption. For the other catalysts, cobalt increased the conversion. Moreover, the solids containing magnesium showed low selectivity to ethene, due to the low acidity of the support, as detected by pyridine chemisorption. The addition of cobalt reduces the ethene selectivity even more and the RCM sample presented the lowest ethene selectivity among the samples.

All catalysts were selective to hydrogen. In addition, they also produced methane, carbon monoxide and carbon dioxide, besides ethene, by side reactions, as shown in Eqs. (5)–(10) [31]. The hydrogen selectivity also changed due to the kind of support. The RM sample led to a high value (51%) which decreased (47%) due to aluminum (RAM sample) and became very low (10%) for RA sample. This suggests that ethanol dehydration is faster than the ethanol reforming to produce hydrogen and, in the presence of acid sites, the first reaction is favored at the expense of the second one. Thus, appreciable quantities of hydrogen are only formed in the absence of acid sites. Cobalt increased the selectivity to hydrogen even more, suggesting again the decrease of acid sites, probably by the coverage of these sites by cobalt. For the RCM sample, this effect is irrelevant, probably due to the absence of acidic sites. A similar behavior is observed regarding carbon monoxide selectivity, the addition of magnesium to the RA sample causes an increase in selectivity, which becomes closer to that based on magnesia.

$$C_2H_5OH \rightarrow C_2H_4 + H_2O \quad (4)$$

$$C_2H_5OH + H_2O \rightarrow 4H_2 + 2CO \quad (5)$$

$$C_2H_5OH \rightarrow CH_3CHO + H_2 \quad (6)$$

Table 2 – Ethanol conversion, selectivities to gaseous products and coke amounts on the spent catalysts during ethanol conversion.

Sample	Ethanol conversion (%)	Selectivity (%)					H_2/CO (molar)	Coke (%)
		H_2	CO	CO_2	C_2H_4	CH_4		
RA	84	10	5.0	2.4	82	0.28	2.2	1.9
RAM	57	47	19	15	9.7	9.5	2.5	3.0
RM	57	51	13	24	3.6	8.6	3.9	1.9
RCA	80	17	5.4	7.4	69	0.43	3.2	2.2
RCAM	70	57	15	12	7.7	8.6	3.8	4.4
RCM	66	53	16	19	1.3	10	3.3	4.6

R: rhodium; C: cobalt; M: magnesia; A: alumina; AM: aluminum and magnesium-based solid.

$$CH_3CHO \rightarrow CO + CH_4 \quad (7)$$

$$C_2H_4 + 2H_2O \rightarrow 2CO + 4H_2 \quad (8)$$

$$CH_4 + H_2O \rightarrow CO + 3H_2 \quad (9)$$

$$CO + H_2O \rightarrow CO_2 + H_2 \quad (10)$$

The catalysts produced different H_2/CO ratios, depending on the kind of support and on the presence of cobalt. For most of the cases, this ratio is higher than the stoichiometric one (Eq. (5)), indicating that hydrogen is also produced by water gas shift reaction, WGSR (Eq. (10)), which is also catalyzed by rhodium and cobalt [7,32]. This is confirmed by the higher values of carbon dioxide selectivity of the samples containing magnesium as compared to alumina-based catalysts. In the last case, the WGSR occurs in a small extension (or not occur), probably because of the high rate of ethanol dehydration. The RA sample showed the lowest ratio which increased due to addition of magnesium (RAM sample) and increased even more for the RM sample. A similar tendency was found for the cobalt-containing catalysts, except for the RCM sample, that showed a value close to the RCA sample. The addition of cobalt increased this ratio, except for the RM sample, probably due to its activity in WGSR [32], as well as in methane steam reforming [33] and ethanol steam reforming [9]. In this case, the methane selectivity is the highest one, suggesting methane reforming did not occur in a large extension.

The magnesium-containing catalysts were selective to methane while magnesium-free catalysts produced very low amounts of this compound. This suggests that the main route of methane production must be from the reactions of acetaldehyde [16]. A previous study [16] has shown that the basic sites catalyze ethanol dehydrogenation to produce acetaldehyde. Additionally, during ethanol steam reforming, acetaldehyde can react by decarbonylation (Eq. (5)) [34] and by steam reforming (Eq. (11)) [16], which increase methane production.

$$CH_3CHO + H_2O \rightarrow CO_2 + CH_4 + H_2 \quad (11)$$

The coke amounts deposited on the catalysts during ethanol reforming are shown in Table 2. Thermodynamic analysis shows that coke production, with graphite structure, is unfavorable when the water to ethanol ratio is equal to three, at temperatures exceeding 227–277 °C [35]. In the present work, however, coke formation may be related to the production of a disordered carbonaceous structure instead of graphite one. Moreover, the thermodynamic analysis cannot predict the composition inside reactor when the system is far from equilibrium [35]. We can see that the lowest amount of coke was deposited on the RA and RM samples, which showed the same amount, the RAM sample showed higher amounts. For the cobalt-containing catalysts, the addition of magnesium led to an increase of coke. These results mean that there is no simple relationship between the coke amount and the basicity of the support and these are not in accordance with several authors [21,33] who claimed that basic solids, like magnesium-containing catalysts, lead to a lower coke deposition as compared to more acidic supports such as alumina. Also, it has been pointed out [20] that ethene is the main precursor of coke during ethanol steam reforming. From the data of Table 2, we can see that magnesium-containing catalysts produced large amounts of methane and carbon monoxide as compared to magnesium-free catalysts, suggesting that coke is mostly produced by Eqs. (12)–(14).

$$CH_4 \rightarrow C + 2H_2 \quad (12)$$

$$2CO \rightarrow CO_2 + C \quad (13)$$

$$CO + H_2 \rightarrow C + H_2O \quad (14)$$

Table 3 shows the yields for all products. Among the catalysts, we can see that the RCAM sample showed the highest hydrogen yield being the most promising catalyst to produce hydrogen by ethanol steam reforming. On the contrary, the RA sample is the worst catalyst showing the lowest hydrogen yield and the highest ethene yield.

Table 3 – Yields for the gaseous products during ethanol conversion over the catalysts.

Sample	Yield (%)				
	H_2	CO	CO_2	C_2H_4	CH_4
RA	8.4	4.2	2.0	69	0.23
RAM	27	11	8.6	5.5	5.4
RM	29	7.4	14	2.0	4.9
RCA	14	4.3	5.9	55	0.3
RCAM	40	10	8.4	5.4	6.0
RCM	35	11	12	0.86	6.6

R: rhodium; C: cobalt; M: magnesia; A: alumina; AM: of aluminum and magnesium-based solid.

4. Conclusion

In studying the effect of support on the properties of rhodium and cobalt-based catalysts for ethanol steam reforming, the use of a hydrotalcite type precursor has been proven to be a suitable route to get active and selective catalysts to produce hydrogen. Heating of magnesium and aluminum-based hydrotalcite produces Mg–Al oxide, which generates rhodium and cobalt catalyst with higher specific surface area and more selective to hydrogen, as compared to alumina or magnesia-based catalysts. The presence of cobalt changes the specific surface area of alumina-based catalysts depending on the presence of magnesium; a similar behavior was noted for magnesium-based catalysts whose specific surface area depends on the presence of aluminum and of cobalt. It also noted that rhodium interacts strongly with the supports in the order: alumina> Mg–Al oxide > magnesia. For all cases, metallic rhodium particles with around 2.4–2.6 nm were formed on the supports but the support based on Mg–Al oxide led to the narrowest particles size distribution; cobalt are supposed to be on the support, affecting its acidity. The catalysts based on alumina led to the highest ethanol conversion, which was associated to ethanol dehydration to produce ethene, instead of ethanol reforming. On the other hand, the magnesium-containing catalysts showed low ethene selectivity and high hydrogen selectivity. The Mg–Al oxide-supported rhodium and cobalt catalyst has shown to be the most promising sample to produce hydrogen by ethanol reforming, showing the highest hydrogen yield and high specific surface area during reaction.

Acknowledgments

JSM thanks CNPq for his graduate scholarship. The authors acknowledge CNPq and FINEP for the financial support.

REFERENCES

[1] Carvalho MFA, Rangel MC. Impacto dos catalisadores automotivos no controle da qualidade do ar. Quím. Nova 2003;26:265–77.
[2] Wang F, Cai W, Provendier H, Schuurman Y, Descorme C, Mirodatos C, et al. Hydrogen production from ethanol steam reforming over Ir/CeO_2 catalysts: enhanced stability by PrOx promotion. Int J Hydrogen Energy 2011;36:13566–74.
[3] Wang C-H, Ho K-F, Chiou JYZ, Lee C-L, Yang S-Y, Yeh C-T, et al. Oxidative steam reforming of ethanol over $PtRu/ZrO_2$ catalysts modified with sodium and magnesium. Catal Comm 2011;12:854–8.
[4] Le Valant A, Garron A, Bion N, Duprez D, Epron F. Effect of higher alcohols on the performances of a $1\%Rh/MgAl_2O_4/Al_2O_3$ catalyst for hydrogen production by crude bioethanol steam reforming. Int J Hydrogen Energy 2011;36:311–8.
[5] Santucci A, Annesini MC, Borgognoni F, Marrelli L, Tosti MRS. Oxidative steam reforming of ethanol over a Pt/Al_2O_3 catalyst in a Pd-based membrane reactor. Int J Hydrogen Energy 2011; 36:1503–11.
[6] Basile A, Pinacci P, Iulianelli A, Broglia M, Drago F, Liguori S, et al. Ethanol steam reforming reaction in a porous stainless steel supported palladium membrane reactor. Int J Hydrogen Energy 2011;36:2029–37.
[7] Peela NR, Kunzru D. Oxidative steam reforming of ethanol over Rh based catalysts in a micro-channel reactor. Int J Hydrogen Energy 2011;36:3384–96.
[8] Liguras DK, Kondarides DI, Verykios XE. Production of hydrogen for fuel cells by steam reforming of ethanol over supported noble metal catalysts. Appl Catal. B 2003;43: 345–54.
[9] Batista MS, Santos RKS, Assaf EM, Assaf JM, Ticianelli EA. High efficiency steam reforming of ethanol by cobalt-based catalysts. J Power Sources 2004;134:27–32.
[10] Busca G, Costantino U, Montanari T, Ramis G, Resini C, Sisani M. Nickel versus cobalt catalysts for hydrogen production by ethanol steam reforming: Ni-Co-Zn-Al catalysts from hydrotalcite-like precursors. Int J Hydrogen Energy 2010;35:5356–66.
[11] Guil-López R, Navarro RM, Peña MA, Fierro JLG. Hydrogen production by oxidative ethanol reforming on Co, Ni and Cu ex-hydrotalcite catalysts. Int J Hydrogen Energy 2011;36: 1512–23.
[12] Padilla R, Benito M, Rodríguez L, Serrano A, Muñoz G, Daza L. Nickel and cobalt as active phase on supported zirconia catalysts for bio-ethanol reforming: influence of the reaction mechanism on catalysts performance. Int J Hydrogen Energy 2010;35:8921–8.
[13] Furtado AC, Alonso CG, Cantão MP, Fernandes-Machado NRC. Bimetallic catalysts performance during ethanol steam reforming: influence of support materials. Int J Hydrogen Energy 2009;34:7189–96.
[14] de la P O'Shea VA, Nafria R, Ramírez de la Piscina P, Homs N. Development of robust Co-based catalysts for the selective H_2-production by ethanol steam-reforming. The Fe-promoter effect. Int J Hydrogen Energy 2008;33:3601–6.
[15] Vizcaíno AJ, Carrero A, Calles JA. Ethanol steam reforming on Mg- and Ca-modified Cu–Ni/SBA-15 catalysts. Catal Today 2009;146:63–70.
[16] Casanovas A, Roig M, de Leitenburg C, Trovarelli A, Llorca J. Ethanol steam reforming and water gas shift over Co/ZnO catalytic honeycombs doped with Fe, Ni, Cu, Cr and Na. Int J Hydrogen Energy 2010;35:7690–8.
[17] Profeti LPR, Ticianelli EA, Assaf EM. Ethanol steam reforming for production of hydrogen on magnesium aluminate-supported cobalt catalysts promoted by noble metals. Appl Catal. A 2009;360:17–25.
[18] Mariño F, Boveria M, Baronetti G, Laborde M. Hydrogen production from steam reforming of bioethanol using $Cu/Ni/K/\gamma\text{-}Al_2O_3$ catalysts. Effect of Ni. Int J Hydrogen Energy 2001; 26:665–8.
[19] Resini C, Delgado MCH, Presto S, Alemany LJ, Riani P, Marazza R, et al. Yttria-stabilized zirconia (YSZ) supported Ni–Co alloys (precursor of SOFC anodes) as catalysts for the steam reforming of ethanol. Int J Hydrogen Energy 2008;33: 3728–35.
[20] Frusteri F, Freni S, Spadaro L, Chiodo V, Bonura G, Donato S, et al. H_2 production for MC fuel cell by steam reforming of ethanol over MgO supported Pd, Rh, Ni and Co catalysts. Catal Commun 2004;5:611–5.
[21] Moura JS, Souza MOG, Rangel MC. Effect of magnesium on the Properties of nickel and lanthanum-based catalysts in steam reforming. Fuel 2008;87:3627–30.
[22] Batista MS, Santos RKS, Assaf EM, Assaf JM, Ticianelli EA. Characterization of the activity and stability of supported cobalt catalysts for the steam reforming of ethanol. J Power Sources 2003;124:99–103.
[23] Cavani F, Trifirò F, Vaccari A. Hidrotalcite-type anionic clays: preparation, properties and applications. Catal Today 1991; 11:173–301.

[24] Ivanova AS. Structure, texture, and acid-base properties of alkaline earth. Oxides, rare earth oxides, and binary oxide systems. Kinet Catal 2005;46:620–33.
[25] Kustrowski P, Sulkowska D, Chmielars L, Rafalska-Lasocha A, Dudek B, Dziembaj R. Influence of thermal treatment conditions on the activity of hydrotalcite-derived Mg-Al oxides in the aldol condensation of acetone. Microporous Mesoporous Mater 2005;78:11–22.
[26] Reddy CR, Bhat YS, Nagendrappa G, Prakash BSJ. Brønsted and Lewis acidity of modified montmorillonite clay catalysts determined by FT-IR spectroscopy. Catal Today 2009;141:157–60.
[27] Araújo GC, Range MC. An environmental Friendly Dopant for the high-temperature shift catalysts. Catal Today 2000;62:201–7.
[28] Arena F, Chuvilin AL, Parmaliana A. Characterization of Li-doped Ni/MgO catalysts. J Phys Chem 1995;99:990–8.
[29] Ruckenstein E, Wang HY. Partial oxidation of methane to synthesis gas over MgO-supported Rh catalysts: the effect of precursor of MgO. Appl Catal. A 2000;198:33–41.
[30] Burch R, Loader PK, Cruise NA. An investigation of the deactivation of Rh/alumina catalysts under strong oxidizing conditions. Appl Catal. A 1996;147:375–94.
[31] Freni S. Rh based catalysts for indirect internal reforming ethanol applications in molten carbonate fuel cells. J Power Sources 2001;94:14–9.
[32] Pereira ALC, Santos NA, Ferreira MLO, Albornoz A, Rangel MC. Effect of cobalt on the activity of iron-based catalysts in water gas shift reaction. Stud Surf Sci Catal 2007;167:225–30.
[33] Araújo GC, Lima S, Rangel MC, La Parola V, Peña MA, Fierro JLG. Characterization of precursors and reactivity of $LaNi_{1-x}Co_xO_3$ for the partial oxidation of methane. Catal Today 2005;107–108:906–12.
[34] Vizcaíno AJ, Carrero A, Calles JA. Hydrogen production by ethanol steam reforming over Cu-Ni supported catalysts. Int J Hydrogen Energy 2007;32:1450–61.
[35] Mas V, Kipreos R, Amadeo N, Laborde M. Thermodynamic analysis of ethanol/water system with the stoichiometric method. Int J Hydrogen Energy 2006;31:21–8.